Organic Electronics 27 (2015) 266–273

Contents lists available at ScienceDirect

Organic Electronics

journal homepage: www.elsevier.com/locate/orgel

The effect of residual palladium catalyst on the performance and stability of PCDTBT:$PC_{70}BM$ organic solar cells

Christopher Bracher [a], Hunan Yi [b], Nicholas W. Scarratt [a], Robert Masters [c], Andrew J. Pearson [a, 1], Cornelia Rodenburg [c], Ahmed Iraqi [b], David G. Lidzey [a, *]

[a] Department of Physics and Astronomy, University of Sheffield, Sheffield, S3 7RH, UK
[b] Department of Chemistry, University of Sheffield, Sheffield, S3 7HF, UK
[c] Department of Materials Science and Engineering, University of Sheffield, Sheffield, S1 3JD, UK

ARTICLE INFO

Article history:
Received 19 June 2015
Received in revised form
14 September 2015
Accepted 2 October 2015

Keywords:
Organic photovoltaics
PCDTBT
Palladium
Lifetime
Stability

ABSTRACT

Palladium (Pd) is commonly used as a catalyst in the polymerisation of conjugated polymers such as poly [N-9′-heptadecanyl-2,7-carbozole-alt-5,5-(4′,7′-di-2-thenyl-2′,1′,3′-benzothiadiazole)] (PCDTBT). Here we explore the effect of residual catalyst on the performance of organic photovoltaic devices (OPVs) based on a PCDTBT:fullerene thin-film blend. We find that as the relative concentration of Pd increases, the power conversion efficiency of the PV is reduced, dropping from 4.55% to 2.42% as the Pd concentration was increased to 2570 ppm (relative to that of the PCDTBT). This reduction in efficiency resulted primarily from a reduction in PV fill factor and shunt-resistance, indicating the presence of current-shunts within the device. Using optical microscopy, laser beam induced current mapping and scanning electron microscopy, we are able to demonstrate that such current shunts are associated with micron-sized aggregates of Pd-containing nanoparticles. We show that the presence of high concentrations of Pd within a PCDTBT OPV contribute to a larger drop in efficiency during the initial 'burn-in' period.

1. Introduction

Organic photovoltaic devices (OPVs) are a promising, low-cost technology for the generation of solar energy. OPVs have potential advantages over other established inorganic technologies as a result of their lower embodied energy, together with enhanced mechanical flexibility, lower weight and the ability to be processed at high volume using a range of high volume printing or coating techniques. The past decade has seen rapid growth and improvements in this field, with optimised devices now having a power conversion efficiency (PCE) [1,2] in excess of 9%; a value at which practical applications are considered commercially viable [3].

A key requirement in the preparation of semiconducting polymers for OPV applications and in the manufacture of solar cells is the need to minimise the presence of contaminants or impurities. Such impurities can increase trap-assisted recombination processes in polymer-fullerene BHJ solar cells, and can have detrimental effects on device efficiency and lifetime [4–6] at concentrations as low as 0.01 wt% (100 ppm) [7]. The conjugated polymers used in OPVs are generally synthesised through Stille [8,9] or Suzuki [10] coupling reactions that are catalysed by palladium (Pd) complexes. These complexes degrade during the polymerisation, creating palladium nanoparticles that bind to the polymer and are difficult to remove [5,11,12]. However, the effect of palladium in a solar cell is dependent on the specific conjugated polymer that is used. For example in solar cells based on poly(p-phenylene vinylene) (PPV), palladium was found to cause shorts [13], and in devices based on poly[[4,8-bis[(2-ethylhexyl)oxy]benzo[1,2-b:4,5-b′]dithiophene-2,6-diyl][3-fluoro-2-[(2-ethylhexyl)carbonyl] thieno [3,4-b]thiophenediyl]]) (PTB7), residual palladium was shown to create traps that assist charge carrier recombination [5].

We have therefore explored the effect of residual palladium catalyst on the performance of OPV devices based on the polymer poly[N-9′-heptadecanyl-2,7-carbozole-alt-5,5-(4′,7′-di-2-thenyl-2′,1′,3′-benzothiadiazole)] (PCDTBT) blended with $PC_{70}BM$. PCDTBT is a semiconducting conjugated polymer that has been widely explored in OPV applications, and is synthesised through the Stille

* Corresponding author.
E-mail address: d.g.lidzey@sheffield.ac.uk (D.G. Lidzey).
[1] Present Address: Optoelectronics Group, Cavendish Laboratory, University of Cambridge, Cambridge, CB3 0HE, UK.

http://dx.doi.org/10.1016/j.orgel.2015.10.001

or Suzuki coupling reactions. Optimised PCDTBT devices have a PCE of around 7.5% [14], an internal quantum efficiency (IQE) approaching 100% and a high degree of photochemical stability [15]. Whilst the effects of the contaminants, $PC_{84}BM$ and TCNQ have been explored in PCDTBT devices [6,16] the effect of residual palladium catalyst in this material has not yet been determined. Here we show that residual Pd content resulting from polymer has a pronounced effect on the efficiency of a PCDTBT-based device, reducing PCE from 4.55% in devices in which the Pd concentration is 0.1 ppm, to 2.42% in devices containing 2570 ppm Pd. Using a variety of techniques, including space charge limited current measurements, optical microscopy, scanning electron microscopy (SEM), laser beam induced current (LBIC) mapping and spatially-resolved photoluminescence measurements, we show that the residual palladium is correlated with the presence of nanoparticle aggregates within the film that create shunts within a device and lead to a reduction in OPV performance. We then show how device stability is affected over 140 h of operation, observing an increase of the fast 'burn-in' of devices containing Pd. Our work highlights the importance of the removal of palladium from PCDTBT, allowing the highest performances and longest operational lifetimes to be achieved.

2. Methods and materials

PCDTBT was synthesised using previously described methods [17]. This 'stock' material had a Pd concentration of 238 ppm as measured by ICP-OES (*vide infra*) and a molecular weight of 15,382 Da. Chlorobenzene (99.95%) was purchased from Sigma–Aldrich and used as received. $PC_{70}BM$ (95% purity) and pre-patterned ITO-coated substrates were purchased from Ossila Ltd. MoO_3 (99.95%) was purchased from Testbourne Ltd, Aluminium (99.99%) and Calcium (99%) were purchased from Sigma Aldrich Ltd.

To achieve a higher Pd concentration in PCDTBT a sample of the stock PCDTBT material (1 g) was added to toluene (50 ml) and was placed into a 250 ml round bottom flask and then heated up to reflux for 3 h under argon. The mixture was cooled down and to this mixture tetraethylammonium hydroxide (16 ml), palladium acetate (21.8 mg) and tri(o-tolyl)phosphine (59.1 mg) were added and then degassed. The mixture was heated to 93 °C overnight and cooled to room temperature. The PCDTBT was precipitated with methanol, collected by filtration and dried under vacuum. This produced a 'Pd polluted' PCDTBT sample having a Pd concentration of 2570 ppm as measured using ICP-OES. The Pd polluted PCDTBT polymer had a molecular weight of 19,070 Da. We speculate that this small apparent increase in molecular weight compared to the stock material (M_n 15,382 Da) most likely resulted from additional coupling reactions during the 'pollution' process, as some of the stock PCDTBT may still have had end-groups bearing either bromide or boronic ester.

To lower the Pd concentration in PCDTBT the stock PCDTBT material (1 g) was dissolved in chloroform (300 ml) to which ammonium hydroxide solution (28% in water) (300 ml) was added. This solution was then heated to reflux for 3 h, and left to cool overnight. The organic phase was separated and then ethylenediamine-tetraacetic acid disodium salt dehydrate (EDTA) (500 mg) was added to the chloroform solution and stirred overnight. Distilled water (300 ml) was added to the solution and the organic phase was separated. The majority of chloroform was then evaporated using a rotary evaporator and the polymer was precipitated with methanol and collected by filtration under nitrogen. A series of Soxhlet extractions were then performed with methanol, acetone, and hexane to remove any inorganic materials that may have still remained within the polymer. A final extraction was performed using chlorobenzene (CB), with polymer precipitated using methanol and collected by filtration and then dried under vacuum. This produced a 'clean' sample of PCDTBT having a Pd concentration of 0.1 ppm as measured using ICP-MS (*vide infra*). The molecular weight of the cleaned PCDTBT was 15,755 Da; a value that is in close agreement with that of the stock material (15,382 Da), indicating that the cleaning process does not result in chain scission. Importantly, the absorption and fluorescence properties of the stock PCDTBT (238 ppm), clean PCDTBT (0.1 ppm) and polluted PCDTBT (2570 ppm) are identical (See Fig. S1 Supplementary Information), indicating that the pollution and cleaning processes did not result in significant degree of chemical oxidation or the production of non-radiative defects.

To explore the role of Pd concentration on device properties, a series of polymer samples were prepared by mixing the clean and polluted PCDTBT samples together at different concentrations. In particular the dry polymer materials were blended in ratios of 5:1, 4:2, 3:3, 2:4 and 1:5, creating a series of samples having assumed Pd concentrations of 0.1, 430, 860, 1290, 1710, 2140 and 2570 ppm.

To measure Pd concentration, samples of interest (typically 5 mg) were digested along with appropriate controls in aqua-regia (6 ml HCl, 2 ml HNO_3) at 150 °C for 2 h. Palladium concentrations were determined using Inductively Coupled Plasma Mass Spectrometry (ICP-MS) (Agilent 7500 spectrometer) for the samples having lower Pd concentrations (<100 ppm), and using Inductively Coupled Plasma Optical Emission Spectrometry (ICP-OES) (Spectro Ciros Vision spectrometer) for the samples having higher Pd concentrations (>100 ppm). For the ICP-MS experiments, data were collected by monitoring the most abundant isotopes of Palladium m/z 105 by using Rhodium m/z 103 as an internal standard, calibrated with a 0–10 ppb synthetic sample solution. For the ICP-MS experiments, data were collected by monitoring at 340.458 nm and 360.955 nm emission lines, calibrated with 0–1 ppm synthetic sample solution. For both ICP-OES and ICP-MS, quartz torches with 2.3 mm diameter injector tubes were employed. To avoid heating and also for easy accessibility, the sample introduction systems were located outside the ICP torch compartment. Synthetic samples containing different acids and acid concentrations were used to evaluate the effect of the acid matrix. These samples were analysed using external calibration and standard addition calibration. These calibration methods were performed in both optical and mass spectrometers.

Solar cells were fabricated on pre-patterned indium tin oxide (ITO) substrates that had been pixelated into individual devices each having an active area of 4.8 mm^2. Substrates were first cleaned by sonication for 5 min in hot deionised (DI) water containing 1% Hellmanex. They were then rinsed in DI water and sonicated in hot DI water followed by another rinse in DI water and a sonication in isopropyl alcohol. Substrates were transferred to a vacuum chamber within a nitrogen-filled glove box. A 10 nm molybdenum oxide (MoO_x) hole-transport layer was then deposited onto the ITO by thermal evaporation at a base pressure of ~10^{-7} mbar. PCDTBT:$PC_{70}BM$ blend films were spin-coated from a CB solution at a 1:4 wt% blend ratio and total concentration of 25 mg ml^{-1} in a nitrogen filled glove box to create films having a thickness of approximately 70 nm. A 5 nm layer of Ca electron-transport layer and a reflective 100 nm layer of Al cathode were then deposited onto the active layer by thermal evaporation (10^{-7} mbar). The devices were finally encapsulated in the glove box using glass slides attached to the device surface with UV curable epoxy (Ossila Ltd.).

Hole only devices were fabricated using the same method as the OPV devices, however a 30 nm thick poly(3,4-ethylenedioxythiophene):polystyrene sulfonate (PEDOT:PSS) hole transport layer was used instead of MoO_x with the Ca/Al cathode

replaced by 70 nm thick layer of Au to block the injection of electrons. Electron only devices retained a Ca/Al cathode, however the MoO_x anode was replaced with a 10 nm thick caesium carbonate layer to block hole injection.

Measurements of device characteristics were conducted under ambient conditions using a Newport 92251A-1000 AM1.5 solar simulator and a Keithley 2400 source meter. The output was calibrated to 100 mW cm^{-2} using an NREL certified silicon reference cell. The area of each device was defined using a 0.0256 cm^2 aperture. OPV lifetime measurements were recorded using an ATLAS Suntest CPS+ with a Xenon 1500 W bulb with IR reducing filters calibrated to 100 mW cm^{-2}. Devices were tested every 30 min without a shadow mask and were held at V_{oc} between measurements.

Laser beam induced current (LBIC) maps were performed using a custom-built setup. A laser diode with a wavelength of 405 nm and a power of 4 mW was focused via a 50× Mitutoyo infinity-corrected objective lens down to a spot size of <5 μm. The sample was mounted on a computer-controlled XY-stage and moved in a raster pattern in 5 μm steps in the X and Y directions. A model SR830 lock in amplifier and a ThorLabs optical chopper were employed to maximise signal.

To explore the nature of the Pd aggregates, 150 nm thick PCDTBT:$PC_{70}BM$ films were spin-coated onto silicon oxide substrates for scanning electron microscopy (SEM). Imaging was performed using a FEI Nova NanoSEM 450 using 5 kV primary beam energy at a working distance of 5 mm, operating in immersion mode. Backscattered electrons (BSE) were used to form an image. The BSE were detected using a solid-state concentric backscatter detector, with all detector segments in operation. Beam current was increased until a strong BSE signal was observed, with no clear damage to the sample being apparent.

Cyclic voltammetry was performed using a Princeton Applied Research Model 263A Potentiostat/Galvanostat. A three electrode system was employed: the reference electrode was Ag/Ag+ (silver wire in 0.01 mol dm^{-3} silver nitrate solution in the electrode solution), the working electrode was a 2 mm diameter smooth platinum disc (area = 3.14 × 10^{-2} cm^2), and the counter electrode was platinum wire. The electrolyte solution was 10 ml of tetrabutylammonium hexafluorophosphate solution in acetonitrile (0.1 mol dm^{-3}). PCDTBT was dissolved in CF (HPLC grade) at 1 mg cm^{-3} concentration and then 0.1 mm^3 was drop cast onto the working electrode prior to measurement. All measurements were performed under argon at (25 ± 2) °C. Ferrocene was used as a reference redox system following IUPAC's recommendation.

To study the PL emission from the devices, a 532 nm diode pumped solid state laser was focused to a 5 μm diameter spot on the sample surface using a 100× microscope lens (numerical aperture of 0.77). The same lens then collected the PL emission and imaged it into a Jobin Yvon Triax 320 spectrometer, with spectra recorded using a nitrogen cooled CCD. A long pass filter with a cut-off of 532 nm was placed before the entrance to the spectrometer to remove background illumination from the laser.

3. Results and discussions

As described in Methods and Materials, a series of PCDTBT samples were created having Pd concentrations of 0.1, 430, 860, 1290, 1710, 2140 and 2570 ppm. Firstly we present the effects of excess Pd on device operation, and then follow this with a discussion of how stability is impacted over 140 h of continuous illumination and operation. Fig. 1 shows the *JV* curves of devices fabricated using PCDTBT:$PC_{70}BM$ blends having 7 different Pd concentrations recorded under AM1.5 irradiation. The average device metrics obtained from the *JV* curves are shown in Table 1, and

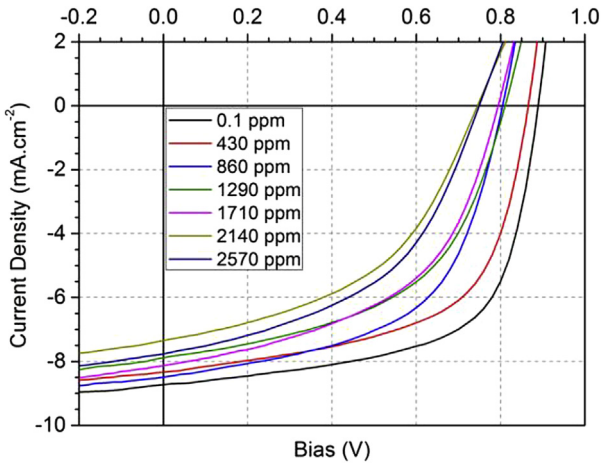

Fig. 1. *JV* curves of the PCDTBT:$PC_{70}BM$ devices fabricated having differing palladium concentrations.

are plotted graphically against Pd concentration in Fig. 2. Here, it can be seen that as the concentration of Pd in the PCDTBT is increased there is a reduction in all device metrics. At the highest Pd concentration explored (2570 ppm) the PCE is reduced by 47% compared to the devices with the lowest palladium content.

As stated above, there is a (~20%) difference between the molecular weight of the 0.1 ppm and 2570 ppm Pd containing polymer samples (being 15,755 Da and 19,070 Da respectively). Previous work demonstrated that the PCE of PCDTBT-based OPVs *increases* as molecular weight *increases*, reaching a maximum for a polymer having a molecular weight of 21.5 kDa (after which point device efficiency reduces) [18]. Here, we observe the opposite effect; efficiency *drops* in devices based on higher molecular weight PCDTBT. This strongly suggests that the reduction in device efficiency observed here can be correlated with increased Pd concentration, rather than changes in the molecular weight of the polymer.

To check whether such reductions in device efficiency result from modification of the electronic-structure of the polymer caused by chemical reactions with Pd, we have used cyclic voltammetry to determine the energetic position of the highest occupied molecular orbital (HOMO) or lowest unoccupied molecular orbital (LUMO) energy levels (Fig. S2). We found that there was a small difference in the HOMO levels (by 0.08 eV) and a negligible

Table 1
Device results showing the average and (peak) values for open circuit voltage, short circuit current density, fill factor, power conversion efficiency, and shunt and series resistance, extracted from the average *JV* curves for PCDTBT containing a range of palladium concentrations.

Pd content	PCE	FF	J_{sc}	V_{oc}	R_{Shunt}	R_{series}
ppm	%	%	mA cm^{-2}	V	Ω cm^2	Ω cm^2
0.1	4.55	60	−8.61	0.89	699	11.8
	(4.91)	(63)	(−8.73)	(0.89)	(740)	(9.8)
430	3.95	57	−8.22	0.85	661	14.5
	(4.27)	(59)	(−8.58)	(0.87)	(692)	(11.5)
860	3.44	53	−8.33	0.78	514	20.4
	(3.79)	(56)	(−8.49)	(0.81)	(585)	(16.3)
1290	2.95	49	−7.91	0.77	416	25
	(3.31)	(52)	(−8.12)	(0.81)	(469)	(20.9)
1710	2.81	47	−8.00	0.77	382	24.5
	(3.25)	(52)	(−8.23)	(0.79)	(417)	(20.2)
2140	2.30	45	−7.26	0.71	377	33.5
	(2.63)	(47)	(−7.97)	(0.75)	(381)	(32.8)
2570	2.42	45	−7.69	0.71	336	29.8
	(2.78)	(48)	(−7.77)	(0.75)	(356)	(28.4)

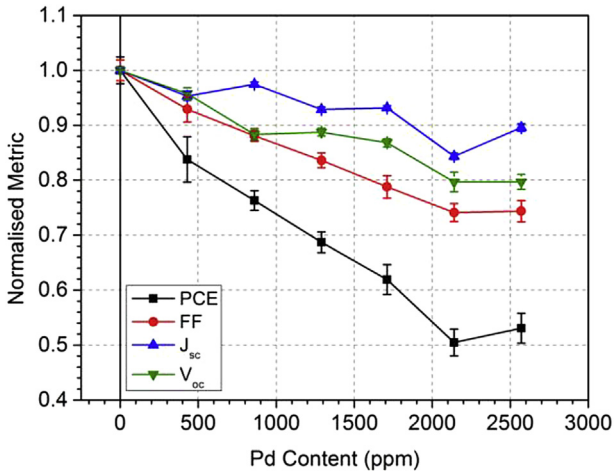

Fig. 2. Changes in device metrics plotted as a function of palladium content, with data normalised to metrics determined from devices containing the lowest concentration of Pd. The lines are a guide for the eye.

difference in LUMO levels between polymers containing either 0.1 ppm or 2570 ppm Pd, indicating that significant changes in electronic structure of the polymer do not occur as a result of Pd contamination. Furthermore, it appears that the Pd does not result in significant changes in the ability of the PCDTBT to transport charge; we have fabricated single carrier devices (see Methods and Materials) in order to determine the hole and electron mobility of PCDTBT:$PC_{70}BM$ blends at the extremes of Pd content (experimental data available in Supplementary Information Fig. S3). Here, we measured a hole mobility of $(3.7 \pm 0.1) \times 10^{-4}$ cm^2 V^{-1} s^{-1} and $(3.2 \pm 0.1) \times 10^{-4}$ cm^2 V^{-1} s^{-1}, and electron mobility of $(1.00 \pm 0.04) \times 10^{-3}$ cm^2 V^{-1} s^{-1} and $(0.99 \pm 0.06) \times 10^{-3}$ cm^2 V^{-1} s^{-1} for the 0.1 ppm and 2570 ppm Pd devices respectively. This suggests that significant changes in hole or electron carrier mobility do not occur as a result of the presence of the Pd catalyst.

We speculate therefore that the observed changes in device efficiency most likely result from an increased density of shunts within the device. Our conclusion is based on the 26% reduction in fill factor (*FF*) that occurs in devices containing 2570 ppm Pd compared to devices with the lowest palladium content. The device shunt (R_{Shunt}) resistance is also dependent on relative Pd concentration, and drops from 699 Ω cm^2 at 0.1 ppm to 335 Ω cm^2 at a Pd concentration of 2570 ppm. Indeed, previous work has also correlated a reduction in R_{Shunt} and FF with an increased density of shorts circuits within an OPV device [13,19].

To confirm the presence of an increased density of short-circuits in devices containing a large fraction of Pd, we have used laser beam induced current (LBIC) mapping. This technique utilises a laser that is focussed to a spot of 5 μm diameter on the device surface and then raster scanned whilst the photocurrent (PC) is recorded. Fig. 3(a–c) show optical micrographs of PCDTBT:$PC_{70}BM$ films that contain 0.1 ppm, 1290 ppm and 2570 ppm Pd respectively, while Fig. 3(d–f) show LBIC maps recorded from the same areas of the film as shown in parts (a) to (c). It can clearly be seen, that as the Pd concentration increases, there is a concomitant increase in the relative density of 'dark' spots in the optical microscope images that are associated with reduced photocurrent in the LBIC images. These current 'cold-spots' have a diameter between 5 and 35 microns, and in many cases are larger than the overall thickness of the active polymer:fullerene layer. In the film containing 0.1 ppm, 1290 ppm and 2570 ppm Pd, we estimate that these current 'cold-spots' appear at a surface density of 51, 195 and 250 mm^{-2} respectively. Considering the relatively large size of these features, together with their relatively high density, we believe that such current-shunts are responsible for the reduced FF and PCE of our OPV devices. It can be seen that the density of such cold-spots does not scale linearly with Pd concentration. The reason for this is currently unclear, however our SEM imaging (*vide infra*) indicates that only a fraction of the available Pd forms large defects responsible for the current cold-spots, with the remainder of the Pd being distributed throughout this film at a level that presumably does not cause a current short. It is also apparent that such cold-spots appear overlaid on a background that has fluctuations in PC that occur over lengths scales of 200 microns. We speculate that long range fluctuations in PC are likely associated with variations in film thickness and polymer:$PC_{70}BM$ mixing ratio.

To probe the nature of such features within films containing a high concentration of Pd, we have performed scanning electron microscopy (SEM) using backscattered electrons as is shown in Fig. 4(a) and (b). Here, we show typical images of two large defects observed in a PCDTBT:$PC_{70}BM$ film containing a 2570 ppm mass fraction of Pd. Here, the image shown in part (a) has a lateral dimension of approximately 1 μm, with the feature in part (b) being more diffuse in nature, having a lateral size of around 6 μm.

We find that in both cases, these defects are composed of a substructure consisting of particles having a size of around 15–45 nm. Imaging using backscattered electrons probes the entire depth of the sample, rather than just the surface, indicating that these particles are distributed *throughout* the defect. We believe such nanoscale particles are composed of Pd; a conclusion confirmed by the fact that the large nuclear charge in Pd nuclei scatters electrons more strongly than the PCDTBT polymer and as such Pd particles produce a larger backscattered signal. Indeed, previous work has shown that palladium nanoparticles bind to conjugated polymers during their synthesis [11] and thus the large aggregates observed in Fig. 4 are likely composed of both PCDTBT and Pd.

A white light optical image of a typical defect is shown in Fig. 5(a). As observed in the SEM images presented above, it can be seen that the defect is characterised by a central Pd-containing core that is surrounded by a polymer:fullerene layer of varying thickness, forming a typical "comet" structure. We have used photoluminescence (PL) spectroscopy to explore the composition of such defects. Here, the PL was excited using light from a 532 nm diode laser focused in a dark-field configuration onto the active layer of an encapsulated device. Emission was collected using a microscope objective lens, with PL spectra being recorded with a spatial resolution of ~5 μm. The PL spectrum recorded from the Pd defect is shown in Fig. 5(d), with PL spectra recorded from two different areas of the film marked with arrows shown in Fig. 5(b) and (c).

It can be seen that the emission from the defect is significantly different from that recorded from other regions of the film. In Fig. 6 we show the PL emission from a PCDTBT film (Pd concentration of 0.1 ppm) and a thin $PC_{70}BM$ film prepared by spin-casting. It appears that PL emitted from the defect is almost identical with that of PCDTBT. The significant similarity between the PL emitted from the defect (shown in Fig. 5(d), and that of PCDTBT indicate that the defects are composed primarily of PCDTBT and Pd, with little to no $PC_{70}BM$ present. In contrast the emission spectra recorded from other points across the film (see Fig. 5(b) and (c)) is similar to that of pure $PC_{70}BM$. This behaviour was observed in films over the entire range of Pd concentrations and is consistent with effective quenching of excitons in PCDTBT, with residual emission occurring from excitons that reside on fullerene aggregates [20].

We speculate therefore that when a Pd-contaminated PCDTBT:$PC_{70}BM$ solution is prepared, some PCDTBT polymer-chains become bound to the Pd nanoparticles. On casting a film, the PCDTBT-Pd aggregate "falls out" of solution before the blend film undergoes vitrification, resulting in the formation of a

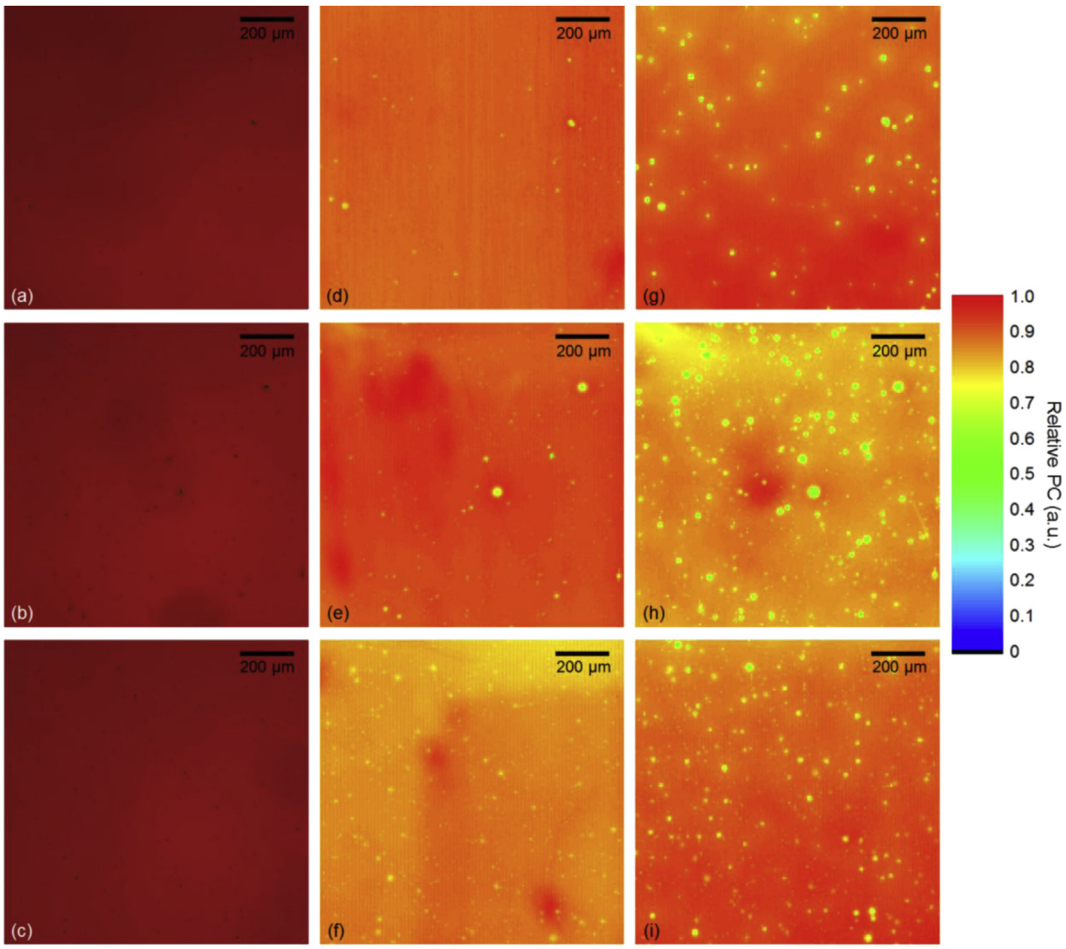

Fig. 3. Parts (a), (b), and (c) are optical microscope images of 0.1 ppm, 1290 ppm, and 2570 ppm Pd PCDTBT:$PC_{70}BM$ films respectively. Parts (d), (e) and (f) are laser beam induced current maps of the films whose images are shown in parts (a), (b), and (c) respectively. Parts (g), (h), and (i) are laser beam induced current maps of the same areas that have been subjected to 140 h of continuous illumination. The maps are normalised individually to the peak value in the image.

mesoscopic polymer-Pd aggregate structure. The composition of such aggregates therefore appears significantly different from that of the bulk film, and contains a significantly reduced fraction of $PC_{70}BM$.

We have shown that the presence of the Pd nanoparticles reduces the efficiency of the OPV devices, principally by reducing device FF as a result of the generation of localised current-shuts. The reduced efficiency of photocurrent generation around the Pd nanoparticles is also likely to result from a reduced probability of exciton dissociation resulting from increased demixing between PCDTBT and $PC_{70}BM$. Indeed, we find that the relative fluorescence emission intensity from films containing a high concentration of Pd is increased (see spectra in Fig. S4).

It is interesting to determine whether such shunts have any

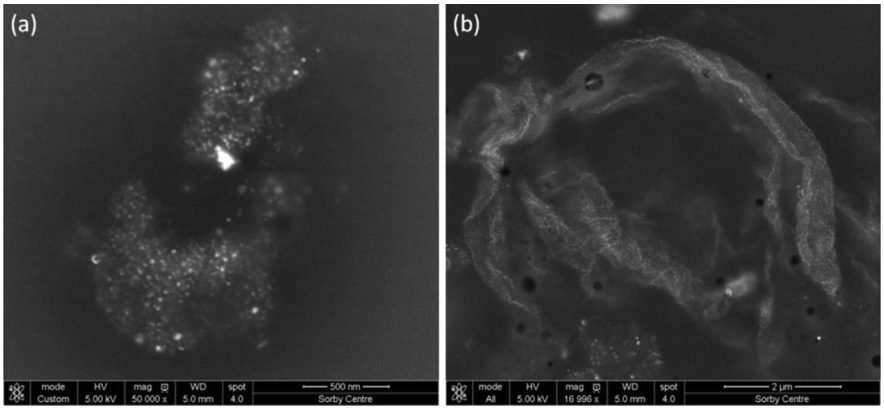

Fig. 4. SEM images of aggregates using backscattered electrons. The width of the image shown in part (a) (left) has a size of ~1 micron, whereas the image part (b) (right) has a width of 6 microns.

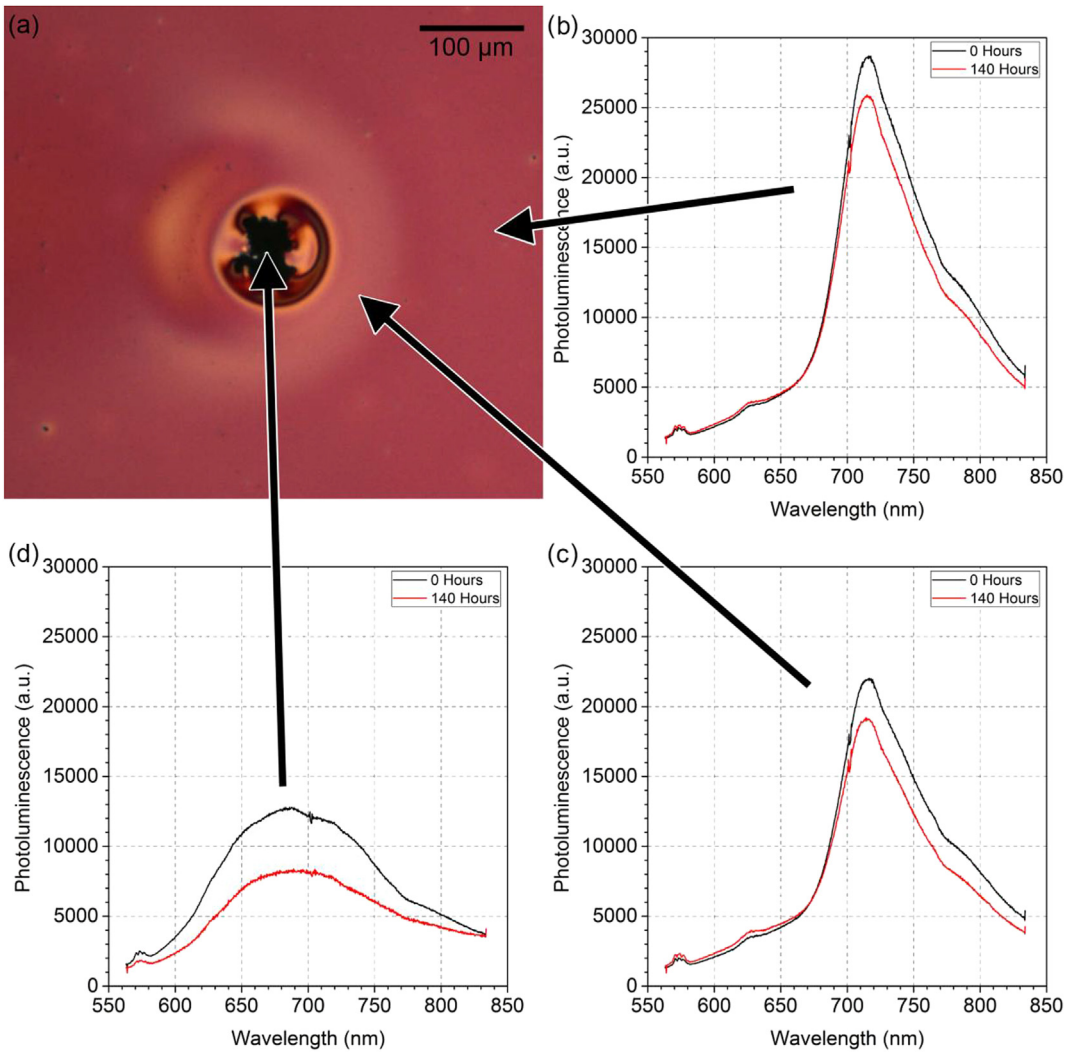

Fig. 5. (a) Optical microscope image of a defect. (b) and (c) PL spectra of the film surrounding the defect before and after 140 h of illumination. (d) PL spectrum of the defect before and after 140 h of illumination.

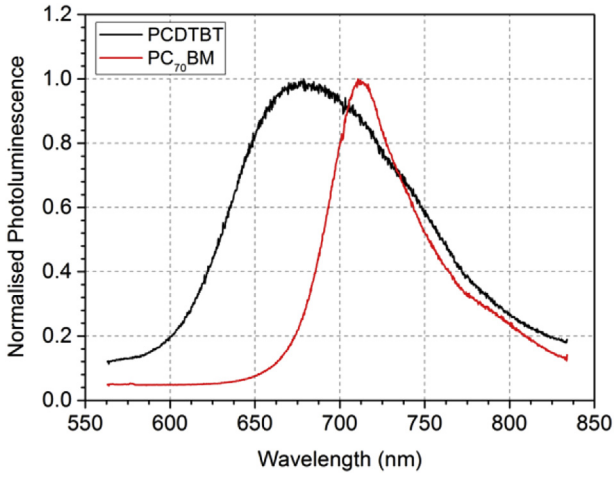

Fig. 6. Normalised photoluminescence spectra for a PCDTBT thin film and $PC_{70}BM$ thin film.

consequence for device operational stability. To explore this issue, we have used a solar simulator (approximating AM1.5 radiation) to track OPV device efficiency over a period of 140 h as shown in Fig. 7. Specifically, Fig. 7(a) shows the relative (normalised) PCE of devices having a varying concentration of Pd as a function of continuous illumination. This decay in PCE is commonly divided into two regions; a 'fast' initial 'burn-in' period (extending here to 60 h) during which the device undergoes rapid degradation. This period is followed by a period in which device degradation is more linear (here shown in Fig. 7(b)). It can be seen that the presence of Pd has a significant effect on the initial 'fast burn-in' period, with devices having a higher Pd concentration generally undergoing a larger initial loss in PCE. (Note the device having the highest Pd concentration (2570 ppm) appears slightly more stable than that having a Pd concentration of 2140 ppm. We do not accord a high degree of significance to this observation and assign this to experimental uncertainty).

From the more linear decay region (60–140 h), (see Fig. 7(b)), we find that the Pd content does not have a significant effect on the stability in the more linear period beyond 'fast burn-in'. Indeed, we use this linear part of the decay-trace to calculate the device T_{80} lifetime, defined as the time taken for the device PCE to drop to 80%

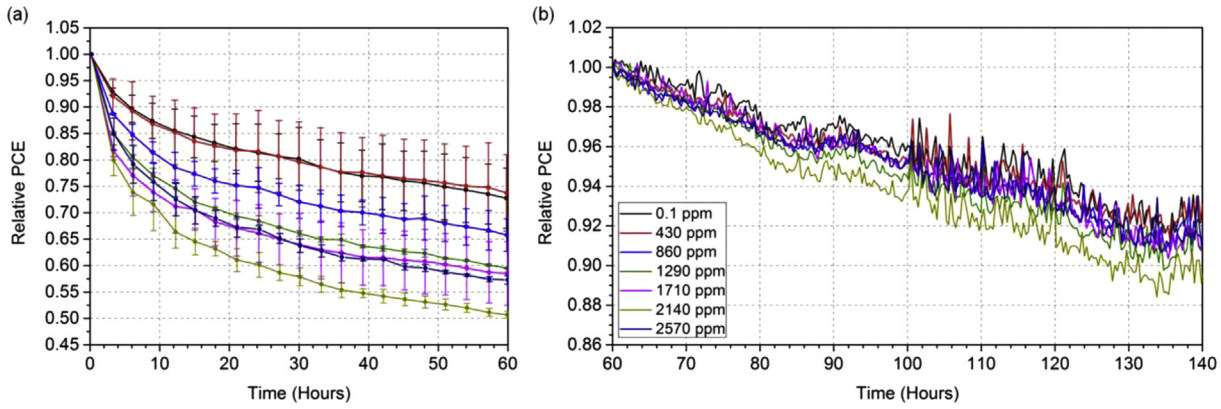

Fig. 7. (a) PCE over 60 h of continuous illumination normalised with respect to the initial PCE, corresponding to the 'burn-in' period. (b) PCE from 60 to 140 h of continuous illumination normalised with respect to the PCE after the 'burn-in' period.

of its PCE determined after the initial 'burn-in' period. Here, we find a T_{80} lifetime of (274 ± 9) hours in devices containing 0.1 ppm Pd, a value similar to that determined for devices containing 2570 ppm (250 ± 21) hours. We summarise this data in Fig. S5. Note that the T_{80} lifetimes determined here are reduced compared to our previous lifetime studies on PCDTBT devices incorporating a MoO_x anode, where a T_{80} lifetime of 650–1000 h was recorded. The apparently shorter lifetimes observed here we believe result from the fact that the degradation of devices was only followed over a relatively short time-scale (140 h), and that some degree of device 'burn-in' was still in progress even at the end of this measurement, making a long-term extrapolation unreliable. Indeed, further measurements are required to explore whether excess Pd concentration plays a role in degradation over time-scales of 1000's of hours. Despite this uncertainty, our results show that devices containing high levels of Pd undergo most rapid degradation in the initial 'fast burn-in' period, with degradation in the period beyond 'burn-in' being less sensitive to the effect of residual palladium catalyst.

To quantify the reduced efficiencies of the Pd containing devices, we plot relative changes in device metrics after 140 h, normalised to values determined at t = 0. This is shown in Supplementary Information in Fig. S6 and Table S1 for a series of devices having different relative concentration of Pd. We find that for devices characterised by a low Pd concentration (0.1–860 ppm), the observed reduction in PCE in aged devices mainly results from a reduction in device *FF* and J_{sc}. For aged devices characterised by higher Pd concentrations (above ~1000 ppm), a strong reduction in device V_{oc} also contributes to a reduction in OPV efficiency.

To explore this process further, we recorded LBIC images of devices that have been aged by exposure to AM1.5 radiation for 140 h (see Fig. 3(g–i)). Here, it is apparent that the number density of cold-spots increases by around 20% in all of the aged devices. From normalised line profiles taken across such defects before and after 140 h of illumination (as shown in Fig. S7) we find some variation in the evolution in shunt structure. Specifically, we find that larger shunts do not change appreciably in their size or depth; however, we find that a population of smaller shunts emerge during the ageing process. Such smaller shunts can grow rapidly in size, increasing in diameter by between 2 and 4 times. The origin of the "new" current shunts observed in the aged devices is as yet unclear. When the polymer:fullerene film is first cast, there exists a 'back-ground' level of Pd nanoparticles that are dispersed within the film that co-exist with the larger nanoparticle aggregates; an example of this can be seen in Fig. S8, where several spots can be seen outside of the defect. We speculate that on ageing such devices under the solar simulator, the nanoparticles are able to undergo slow thermally-assisted diffusion and aggregation within the film (perhaps assisted by the field within the device), eventually reaching a size whereby they are also able to act as current shunts; a process likely to contribute to the observed loss in PCE.

To explore whether the photoactive material is modified by its proximity to a Pd-containing defect, we also recorded PL spectra at different distances (from 0 to 250 microns) from a single aggregate after 140 h of AM1.5 irradiation, as shown in Fig. 5(b–d). Interestingly, we find that the PL emission spectra do not change after the ageing process, however they all undergo a decrease in intensity (by around 10% for the film, 30% for the defect), an observation consistent with photo-oxidation [21].

Our measurements suggest therefore that there are two contributory factors to the loss in device efficiency during the 'fast burn-in' period. Firstly, the appearance of additional Pd defects acting as current shunts are likely to reduce device efficiency. Secondly however, the observed reduction in the PL emission intensity that is observed in regions far from the Pd defect and accompanied by a reduction of V_{oc} and FF indicates an accompanying oxidation process that is consistent with the formation of sub-bandgap states. It has been shown previously that the generation of such states is a primary mechanism for the 'burn-in' loss of PCDTBT:$PC_{70}BM$ solar cells [22].

4. Conclusions

We have explored the effect of residual palladium-catalyst left over from the synthesis of the polymer PCDTBT on its efficiency when fabricated into a polymer:fullerene solar cell. We find that the Pd has a significant effect of device efficiency, with PCE reduced by almost 50% from 4.55% to 2.42% due to the presence of 2570 ppm of Pd (relative to the mass of PCDTBT). We attribute this to the presence of the Pd that self-assembles into 15 nm nanoparticles that are then bound by the PCDTBT polymer into larger sized aggregates (>10 μm). We have used laser beam photocurrent mapping to demonstrate that such aggregates are associated with reduced photocurrent within the device and thus act as short-circuits that result in additional leakage pathways between the anode and cathode that conduct charge. On ageing the devices, a number of additional current shunts appear; an effect that we believe contributes to a loss in device efficiency. Our measurements thus highlight the need to remove Pd from PCDTBT after polymer synthesis, as it is responsible for both reduced device efficiency and enhanced device degradation.

Acknowledgements

The authors would like to thank Dr. Darren C. Watters for useful discussions and Dr. Edward S. R. Bovill for assistance with the lifetime measurements. We thank the UK EPSRC for supporting this research through research grants EP/I028641/1 "Polymer/fullerene photovoltaic devices: new materials and innovative processes for high-volume manufacture" and EP/J017361/1 "Supergen Supersolar Hub". C.B. and R.M. thank the University of Sheffield for funding their studentships via the Shine Doctoral Training Centre.

Appendix A. Supplementary data

Supplementary data related to this article can be found at http://dx.doi.org/10.1016/j.orgel.2015.10.001.

References

[1] Z. He, C. Zhong, S. Su, M. Xu, H. Wu, Y. Cao, Enhanced power-conversion efficiency in polymer solar cells using an inverted device structure, Nat. Photonics 6 (2012) 591–595, http://dx.doi.org/10.1038/NPHOTON.2012.190.

[2] M.A. Green, K. Emery, Y. Hishikawa, W. Warta, E.D. Dunlop, Solar cell efficiency tables (version 43), Prog. Photovolt. Res. Appl. 22 (2014) 1–9, http://dx.doi.org/10.1002/pip.

[3] J.R. Sheats, Manufacturing and commercialization issues in organic electronics, J. Mater. Res. 19 (2011) 1974–1989, http://dx.doi.org/10.1557/JMR.2004.0275.

[4] W.R. Mateker, J.D. Douglas, C. Cabanetos, I.T. Sachs-Quintana, J. a Bartelt, E.T. Hoke, et al., Improving the long-term stability of PBDTTPD polymer solar cells through material purification aimed at removing organic impurities, Energy Environ. Sci. 6 (2013) 2529, http://dx.doi.org/10.1039/c3ee41328d.

[5] M.P. Nikiforov, B. Lai, W. Chen, S. Chen, R.D. Schaller, J. Strzalka, et al., Detection and role of trace impurities in high-performance organic solar cells, Energy Environ. Sci. 6 (2013) 1513, http://dx.doi.org/10.1039/c3ee40556g.

[6] L. Kaake, X.-D. Dang, W.L. Leong, Y. Zhang, A. Heeger, T.-Q. Nguyen, Effects of impurities on operational mechanism of organic bulk heterojunction solar cells, Adv. Mater. 25 (2013) 1706–1712, http://dx.doi.org/10.1002/adma.201203786.

[7] W.L. Leong, G. Hernandez-Sosa, S.R. Cowan, D. Moses, A.J. Heeger, Manifestation of carrier relaxation through the manifold of localized states in PCDTBT:PC60BM bulk heterojunction material: the role of PC84BM traps on the carrier transport, Adv. Mater. 24 (2012) 2273–2277, http://dx.doi.org/10.1002/adma.201104192.

[8] D. Milstein, J.K. Stille, A. General, Selective, and facile method for ketone synthesis from acid chlorides and organotin compounds catalyzed by palladium, J. Am. Chem. Soc. 100 (1978) 3636–3638.

[9] B. Carsten, F. He, H.J. Son, T. Xu, L. Yu, Stille polycondensation for synthesis of functional materials, Chem. Rev. 111 (2011) 1493–1528, http://dx.doi.org/10.1021/cr100320w.

[10] A. Suzuki, Organoborates in new synthetic reactions, Acc. Chem. Res. 15 (1982) 178–184.

[11] K.T. Nielsen, K. Bechgaard, F.C. Krebs, Removal of palladium nanoparticles from polymer materials, Macromolecules 38 (2005) 658–659, http://dx.doi.org/10.1021/ma047635t.

[12] P. a. Troshin, D.K. Susarova, Y.L. Moskvin, I.E. Kuznetsov, S. a. Ponomarenko, E.N. Myshkovskaya, et al., Impedance measurements as a simple tool to control the quality of conjugated polymers designed for photovoltaic applications, Adv. Funct. Mater. 20 (2010) 4351–4357, http://dx.doi.org/10.1002/adfm.201001308.

[13] F.C. Krebs, B. Nyberg, M. Jørgensen, A.B.S. Energy, M. Sol, Influence of residual catalyst on the properties of conjugated polyphenylenevinylene materials : palladium nanoparticles and poor electrical performance, Chem. Mater. 16 (2004) 1313–1318.

[14] D.H. Wang, J.K. Kim, J.H. Seo, I. Park, B.H. Hong, J.H. Park, et al., Transferable graphene oxide by stamping nanotechnology: electron-transport layer for efficient bulk-heterojunction solar cells, Angew. Chem. Int. Ed. Engl. 52 (2013) 2874–2880, http://dx.doi.org/10.1002/anie.201209999.

[15] S.H. Park, A. Roy, S. Beaupré, S. Cho, N.E. Coates, J.S. Moon, et al., Bulk Heterojunction solar cells with internal quantum efficiency approaching 100%, Nat. Photonics 3 (2009) 297–302. http://www.nature.com/nphoton/journal/v3/n5/abs/nphoton.2009.69.html.

[16] S.R. Cowan, W.L. Leong, N. Banerji, G. Dennler, A.J. Heeger, Identifying a threshold impurity level for organic solar cells: enhanced first-order recombination via well-defined pc84bm traps in organic bulk heterojunction solar cells, Adv. Funct. Mater. 21 (2011) 3083–3092, http://dx.doi.org/10.1002/adfm.201100514.

[17] N. Blouin, a. Michaud, M. Leclerc, A low-bandgap poly(2,7-carbazole) derivative for use in high-performance solar cells, Adv. Mater. 19 (2007) 2295–2300, http://dx.doi.org/10.1002/adma.200602496.

[18] J.W. Kingsley, P.P. Marchisio, H. Yi, A. Iraqi, C.J. Kinane, S. Langridge, et al., Molecular weight dependent vertical composition profiles of PCDTBT:PC71BM blends for organic photovoltaics, Sci. Rep. 4 (2014) 1–7, http://dx.doi.org/10.1038/srep05286.

[19] S. Günes, H. Neugebauer, N.S. Sariciftci, Conjugated polymer-based organic solar cells, Chem. Rev. 107 (2007) 1324–1338, http://dx.doi.org/10.1021/cr050149z.

[20] T. Wang, A.J. Pearson, A.D.F. Dunbar, P. a Staniec, D.C. Watters, H. Yi, et al., Correlating structure with function in thermally annealed PCDTBT: PC70BM photovoltaic blends, Adv. Funct. Mater. 22 (2012) 1399–1408, http://dx.doi.org/10.1002/adfm.201102510.

[21] E. Bovill, N. Scarratt, J. Griffin, H. Yi, A. Iraqi, A.R. Buckley, et al., The role of the hole-extraction layer in determining the operational stability of a polycarbazole:fullerene bulk-heterojunction photovoltaic device, Appl. Phys. Lett. 106 (2015) 073301, http://dx.doi.org/10.1063/1.4909530.

[22] C.H. Peters, I.T. Sachs-Quintana, W.R. Mateker, T. Heumueller, J. Rivnay, R. Noriega, et al., The mechanism of burn-in loss in a high efficiency polymer solar cell, Adv. Mater. 24 (2012) 663–668, http://dx.doi.org/10.1002/adma.201103010.